SUPPORTING INFORMATION FOR:

Radical Doped Hole Transporting Material for High-Efficiency and Thermal Stable Perovskite Solar Cells

*Yuxi Zhang,[1,2] Bo Huang,[2] Min Hu,[3] Boer Tan,[4] Fuzhi Huang,[2,5] Yi-Bing Cheng,[2,5] Alexandr N. Simonov,[6] Jianfeng Lu[1,2]**

[1] State Key Laboratory of Silicate Materials for Architectures, Wuhan University of Technology, 430070 Wuhan, China

[2] Foshan Xianhu Laboratory of the Advanced Energy Science and Technology Guangdong Laboratory, Foshan 528216, China

[3] School of Electronic and Electrical Engineering, Hubei Province Engineering Research Center for Intelligent Micro-nano Medical Equipment and Key Technologies, Wuhan Textile University, Wuhan 430200, P. R. China.

[4] Department of Chemical and Biological Engineering, ARC Centre of Excellence for Exciton Science, Monash University, Victoria 3800, Australia

[5] State Key Laboratory of Advanced Technology for Materials Synthesis and Processing, Wuhan University of Technology, Wuhan 430070, P. R. China

[6] School of Chemistry, Monash University, Victoria 3800, Australia

EXPERIMENTAL

Materials

Cesium iodide (CsI), isobutylamine bromide (i-BABr), poly(3-hexylthiophene-2,5-diyl)(P3HT), poly(triaryl amine) (PTAA) were purchased from Xi'an Polymer Light Co., Ltd. Methylammonium (MA^+) bromide, poly(4-butyl-N,N-diphenylaniline) (poly-TPD) was purchased from Luminescence Technology Corp. Lead iodide (PbI_2) was purchased from TCI. Formamidinium (FA^+) iodide was purchased from Greatcell Solar Materials Pty Ltd. 1,1,2,2-Tetrachloroethane (TeCA) was purchased from Adamas Pharmaceuticals, Inc. 2,2',7,7'-tetrakis (N,N-di-p-methoxyphenylamino)-9,9-spirobifluorene (*spiro*-OMeTAD) was purchased from Shenzhen Feiming Science and Technology Co., Ltd. Other materials were purchased from Alfa-Aesar and Sigma Aldrich and used without any further purification.

Device fabrication

FTO substrates preparation: The FTO glass was firstly etched using a femtosecond laser machine. Then it was cleaned through ultrasonic cleaning by detergent, pure water, and ethyl alcohol for 20 min, respectively. After drying by dry-air blowing, it was treated by Ultraviolet ozone (UVO) for 15 min before use.

Electron transport layer (ETL) fabrication: SnO_2 was deposited onto clean FTO glass substrate by a chemical bath deposition (CBD) method according to reports.[1] 5 g urea was dissolved into 400 mL deionized water, followed by the addition of 100 μL mercaptoacetic acid and 5 mL HCl (37 wt%), and then 1.096 g $SnCl_2 \cdot 2H_2O$ was dissolved in the solution (~ 0.012 M). The solution was stored in a fridge before use. The as-cleaned FTO glass was soaked into the diluted $SnCl_2 \cdot 2H_2O$ solution (~ 0.002 M) for 2.5 hours at 90 ℃. Then it was washed by deionized water, dried by blowing air, and followed by the annealing at 180℃ for 1 hour. Before device fabrication, all the SnO_2/FTO substrates were treated by UVO for 15 min.

Further, perovskite and HTL deposition procedures were undertaken inside a N_2/Ar-filled glovebox.

Perovskite layer: The $Cs_{0.05}FA_{0.79}MA_{0.16}PbBr_{0.51}I_{2.49}$ mixed perovskite precursor was prepared by dissolving 1.4 M mixture of lead salts composed of 0.85 PbI_2 and 0.15 $PbBr_2$, and 1.3 M organic cation that are composed of 0.85 FAI and 0.15 MABr in the a mixed solvent of N,N-dimethylformamide solution (DMF)/ Dimethyl sulfoxide (DMSO) (4:1, vol.), and adding 34 μL CsI (pre-dissolved as a 2 M stock solution in DMSO) to achieve the desired perovskite solution. The perovskite absorber was deposited onto the UVO-processed SnO_2 substrates (UV illuminated for 10 min) by spin-coating a 25 μL mixed perovskite solution at 6000 rpm for 30 s with 1000 rpm s^{-1} ramp, 120 μL anti-solvent of ethyl acetate was dropped at the last 5th second. The films were then annealed at 120 °C for 45 min.

Further, all the achieved perovskite films were treated with a 15 mM i-BABr/IPA solution at 4000 rpm for 20 s with 4000 rpm s^{-1} ramp, and annealed at 100 ℃ for 5 min.

Hole transport layer (HTL) fabrication: Convention HTL precursor solution was prepared by dissolving 73 mg *spiro*-OMeTAD in 1 mL chlorobenzene. The molar ratios of additives for *spiro*-OMeTAD were 0.55, 3.47 and

0.09 for LiTFSI, *t*BP and FK209, respectively.

Solutions of *spiro*-OMeTAD in TeCA were prepared by dissolving 24.3-73mg of *spiro*-OMeTAD in 1mL TeCA (20-60mM). Whenever required, varied amounts (0-120 mol.% with respect to *spiro*-OMeTAD) of BPO or nBu$_4$NPF$_6$ (tetrabutylammonium hexafluorophosphate) were added from their 1.6 and 1.0 M stock solutions, respectively. The latter were prepared by dissolving 0.077g BPO or 0.077g nBu$_4$NPF6 in 200 µL TeCA.

For deposition, the required *spiro*-OMeTAD solution was spin-coated onto the perovskite films at 3000 rpm for 30s (3000 rpm s^{-1} ramp).

As a final step of the device fabrication, 80-nm thick gold layer was deposited by using thermal evaporation.

Module fabrication:

P1, P2 and P3 scribing etch using a femtosecond laser machine of series-connected modules. The FTO glass was firstly etched form P1 lines. After the deposition of the *spiro*-OMeTAD film, the sample was re-etched to form P2 lines. Finally, it formed effective series-connected modules by etching the Au to form P3 lines.

Characterization

The perovskite and HTL films were investigated using field-emission scanning electron microscope (SEM) (S-4800, Hitachi, Japan), atomic force microscope (AFM) (NX10, Park, Korea), Ultraviolet photoelectron spectroscopy (UPS), X-ray photoelectron spectroscopy (XPS) (ESCALAB 250Xi). UV-Vis spectrometer (lambda 750 S, PerkinElmer), X-ray diffractometer (XRD, D8 Advance). PL, TRPL, time-resolved confocal PL microscopy (Micro Time 200, PicoQuant GmbH), respectively.

The current density-voltage (*J-V*) curves of these PSCs were measured using a Keithley 2400 source meter in the room environment. The light source was a solar simulator (Oriel 94023 A, 300 W) matching AM 1.5G. The intensity of the light was 100 mW cm^{-2} calibrated by a standard silicon reference solar cell (Oriel, VLSI standards). The *J-V* scans were recorded at 10 mV steps in forward (–0.1 V→1.2 V) and reverse (1.2 V→–0.1 V) directions. All the devices were tested using a black metal aperture with a defined active area of 0.16 cm^2 for the small devices.

The conductivity normalized to the device geometry was calculated according to the equation

$$\sigma = \frac{I \quad d}{v(2n-1)lh}$$

where I is the measured current, V is the applied voltage, d is the spacing between adjacent electrodes, n is the number of finger pairs, l is the length of the overlap area of the fingers, and h is the thickness of the HTM film. The thickness of the different doped sample was determined by cross-sectional SEM images. CB-**S** and CB-doped-**S** film thickness is 200nm, TeCA-**S**, TeCA-BPO-**S** and TeCA-BPO-PF$_6$-**S** film thickness was 70nm.

Thermal stability test: all devices are placed in a glass petri dish which located in an 85℃ oven (environmental conditions: 20 ± 5 ℃, 15 ± 5% relative humidity). All the devices are cooled down before each test.

SUPPLEMENTARY DATA.

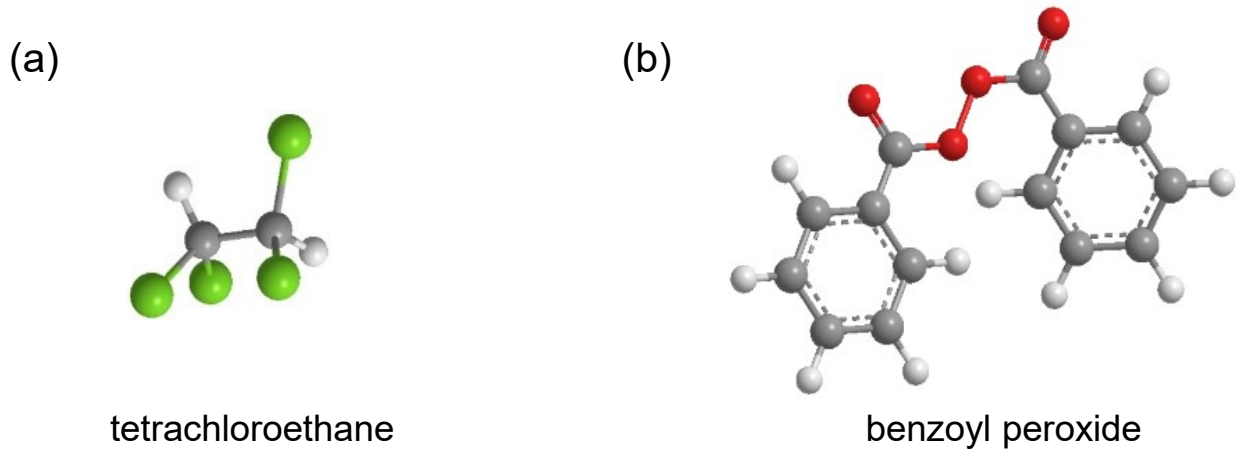

Figure S1. Chemical structures of (a) 1,1,2,2-tetrachloroethane (TeCA), (b) benzoyl peroxide (BPO).

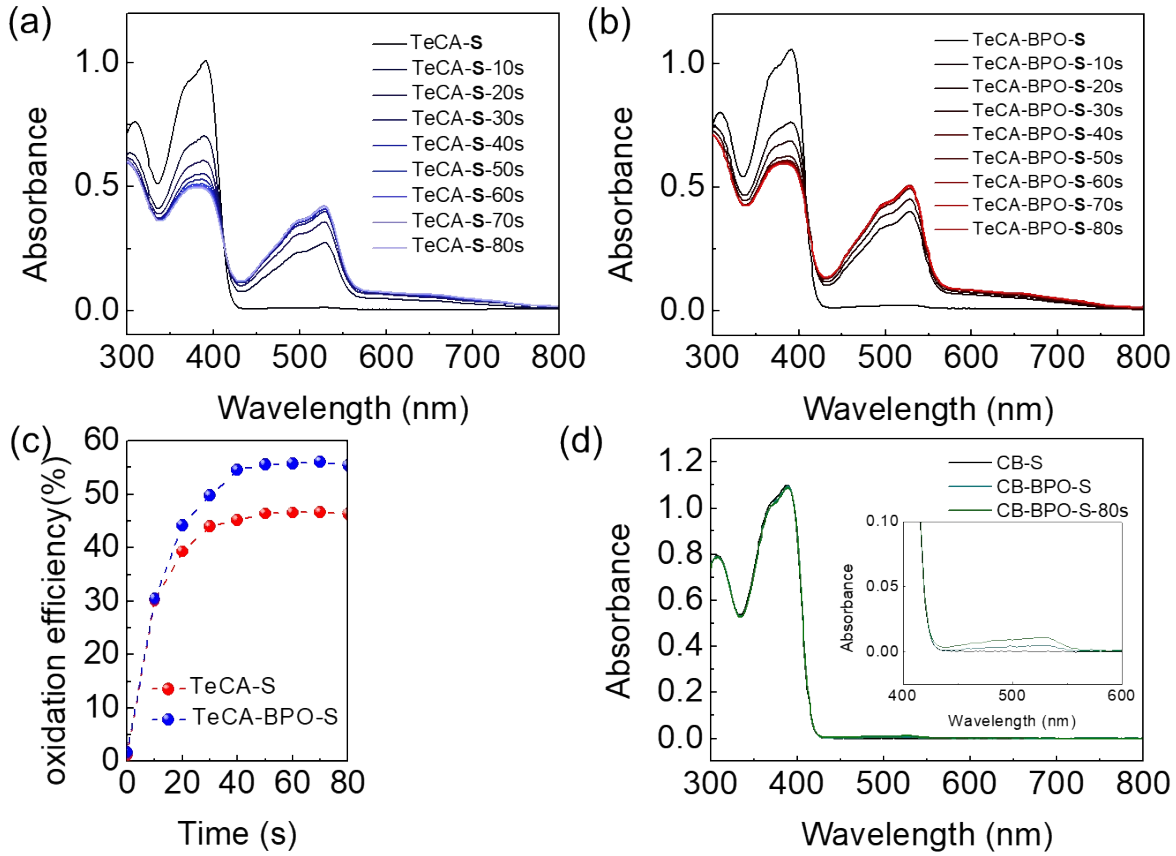

Figure S2. Evolution of the UV−Vis absorption spectra of 2.6×10^{-5} M *spiro*-OMeTAD solutions in (a) TeCA and (b) TeCA with 90 mol.% (with respect to *spiro*-OMeTAD) BPO under 1-sun illumination, and (c) corresponding changes in the amount of [*spiro*-OMeTAD]$^{\bullet+}$ (mol.% with respect to the initial *spiro*-OMeTAD^{0} amount). (d) UV-Vis absorption spectra of *spiro*-OMeTAD dissolved in CB and containing 90 mol.% of BPO (with respect to *spiro*-OMeTAD); for the latter solution, data are shown before and 80 s of irradiation under 1-sun. The inset shows the enlarged spectra of the oxidized *spiro*-OMeTAD peak at around 528 nm.

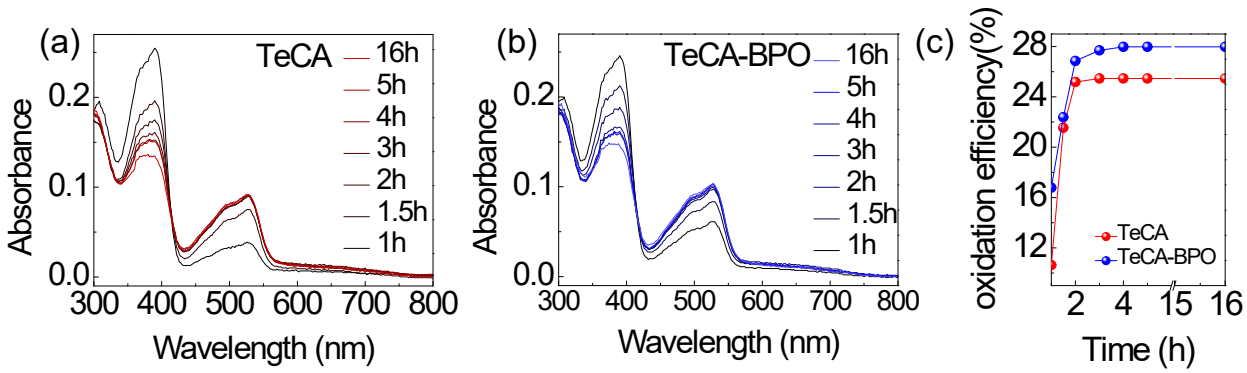

Figure S3. Evolution of the UV−Vis absorption spectra *spiro*-OMeTAD solutions in (a) TeCA and (b) TeCA with 90 mol.% (with respect to *spiro*-OMeTAD) BPO under 0.014-sun illumination. (c) corresponding changes in the amount of $[\text{spiro-OMeTAD}]^{\bullet+}$ (mol.% with respect to the initial spiro-OMeTAD^{0} amount).

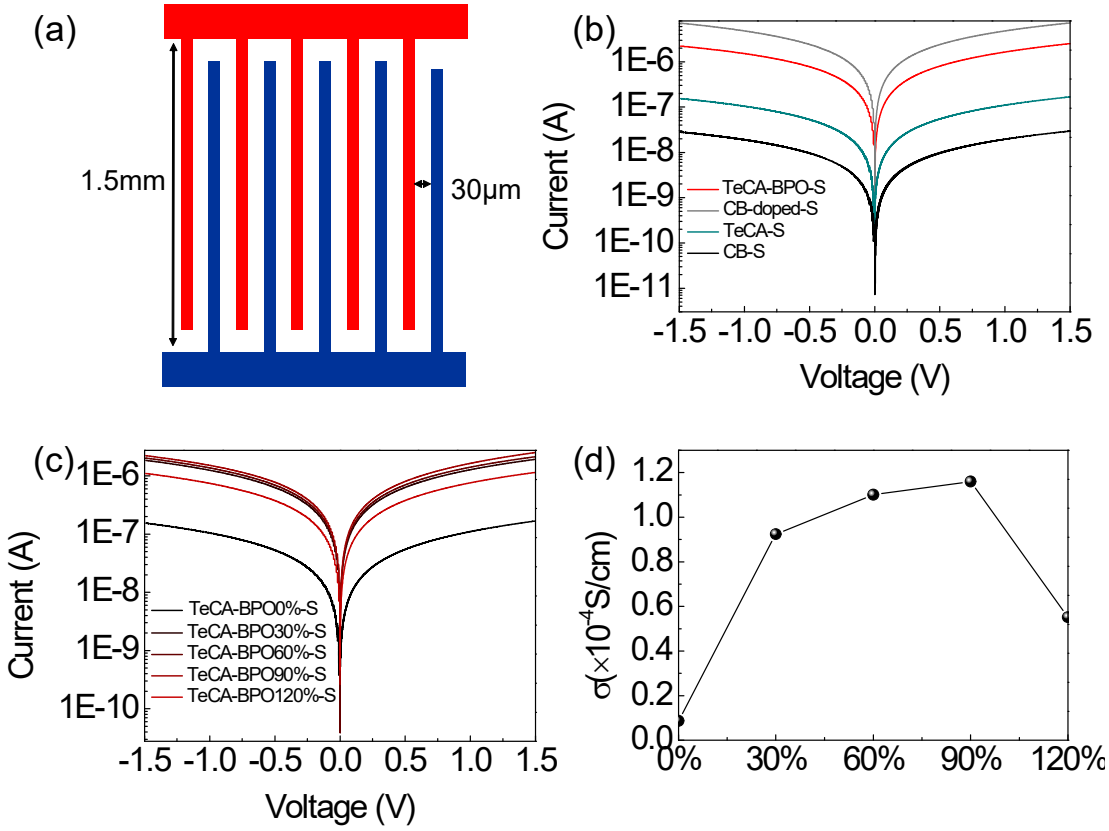

Figure S4. (a) Schematic illustration of the gold IDAs used for conductivity measurements. The distance between adjacent fingers is $d = 30$ μm, the length of the fingers is $l = 1.5$ mm, the number of finger pairs is 75. (b) I-V characteristics of spin-coated different HTM films (c) I-V characteristics of spin-coated *spiro*-OMeTAD films doped with different molar concentrations of BPO relative to *spiro*-OMeTAD. (d) Conductivity derived from (c) as a function of BPO content.

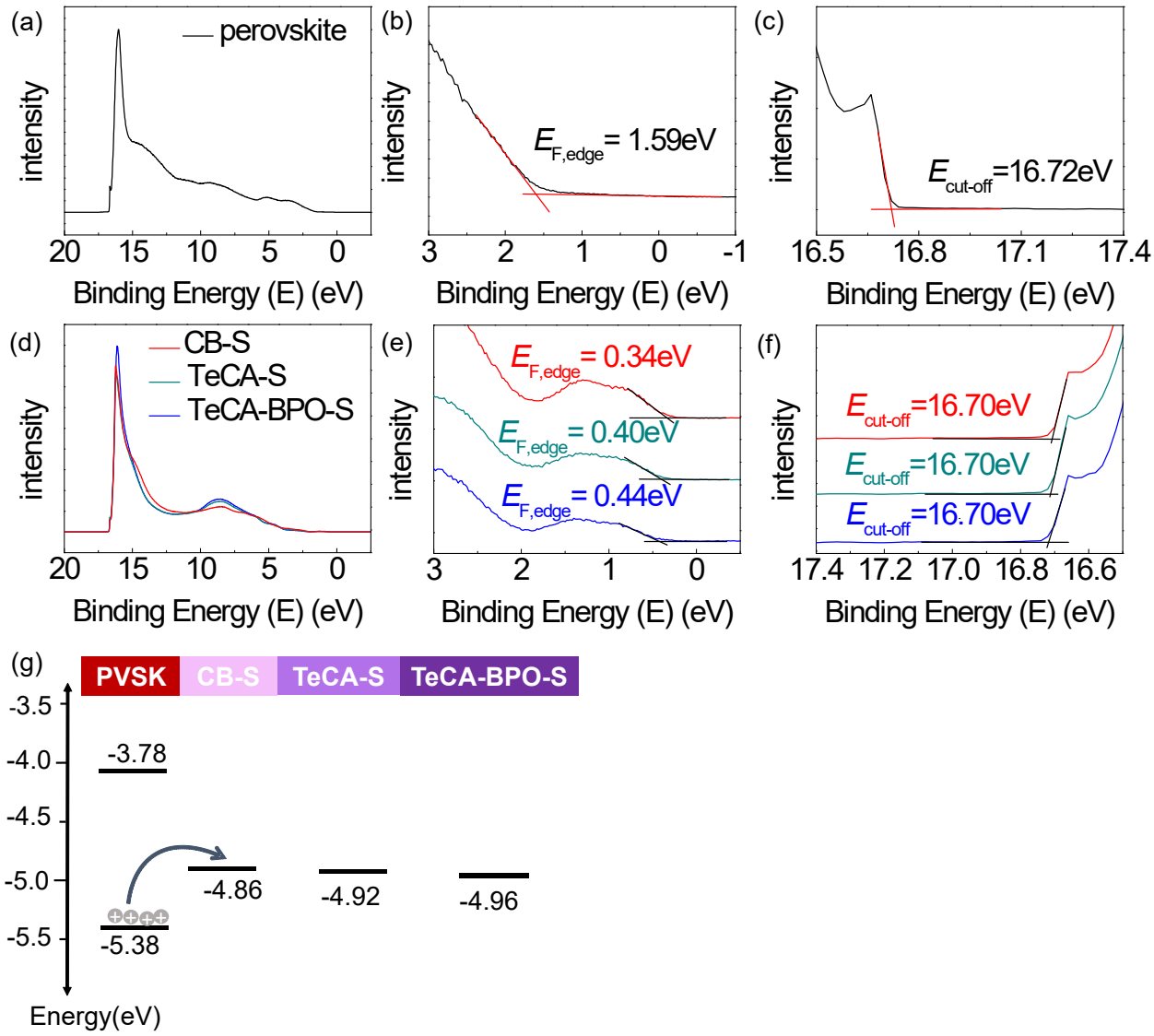

Figure S5. UPS spectra of the $Cs_{0.05}FA_{0.79}MA_{0.16}PbBr_{0.51}I_{2.49}$ perovskite (*dark*), unadulterated *spiro*-OMeTAD (*red*), TeCA (*dark cyan*) and TeCA-BPO (*blue*) showing (a, d) full range, (b, e) the cut-off energy ($E_{cut-off}$), and (c, f) Fermi edge ($E_{F,edge}$). (g) Energy band schematic for $Cs_{0.05}FA_{0.79}MA_{0.16}PbBr_{0.51}I_{2.49}$ and different HTLs.

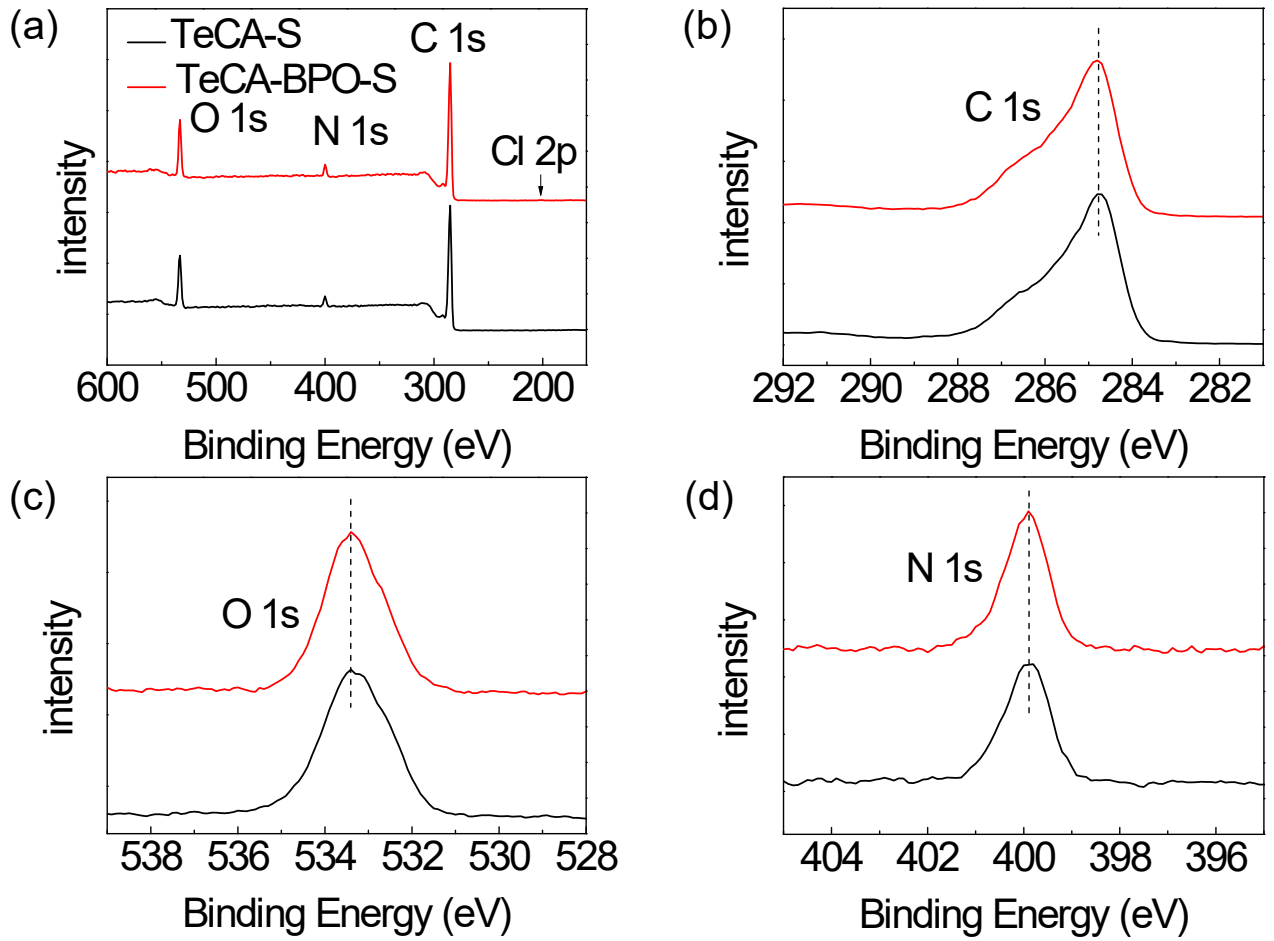

Figure S6. XPS analysis of the *spiro*-OMeTAD flims doped using TeCA (*black*) and TeCA-BPO combination (*red*) (a) survey, (b) C 1s, (c) O 1s and (d) N 1s spectra. All data were corrected to the C 1s peak at 284.8eV. The N: Cl ratio from XPS is 17:1.

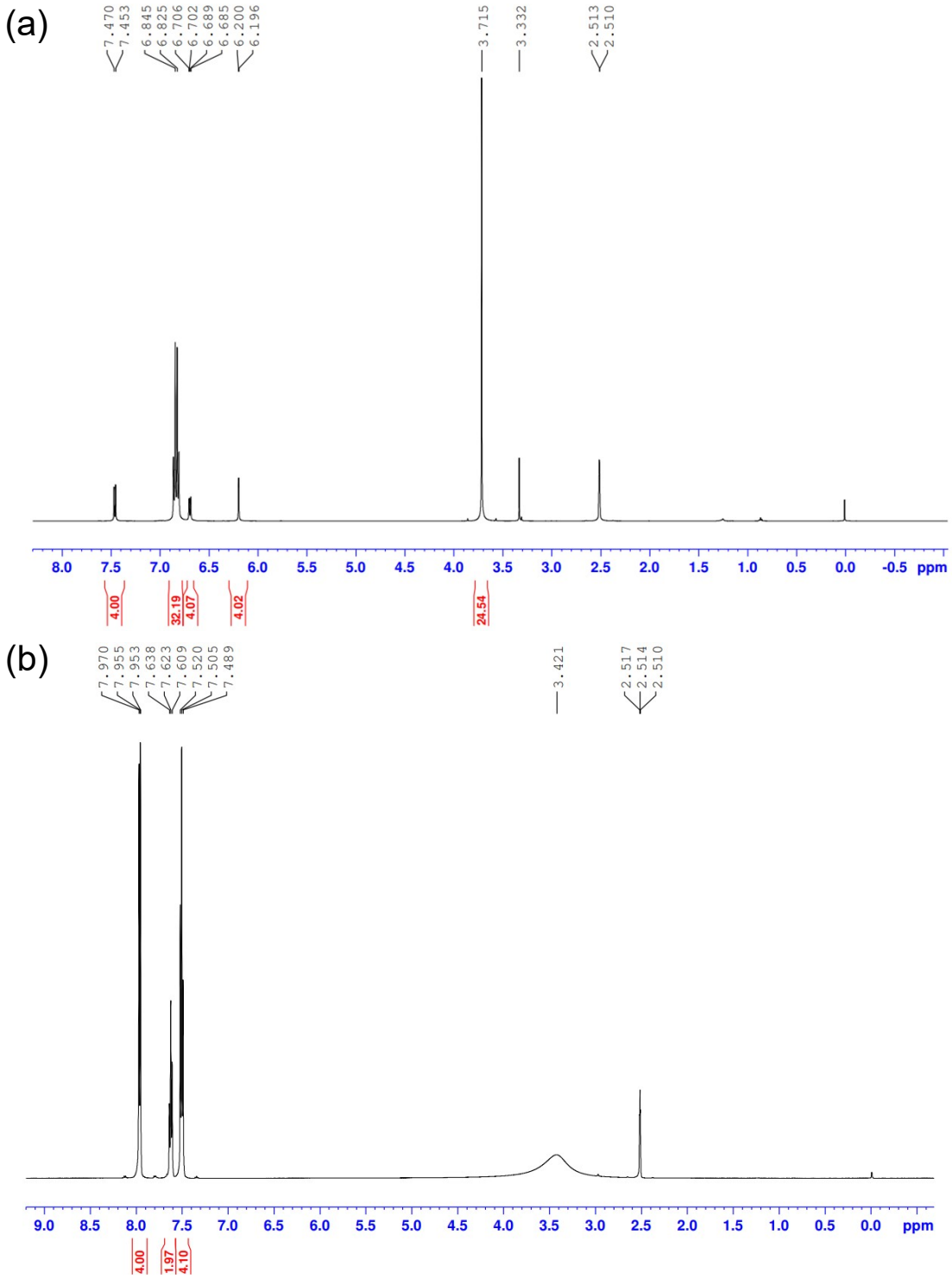

Figure S7. ^{1}H NMR spectra of (a) pure *spiro*-OMeTAD and (b) pure BPO dissolved in d_6-DMSO.

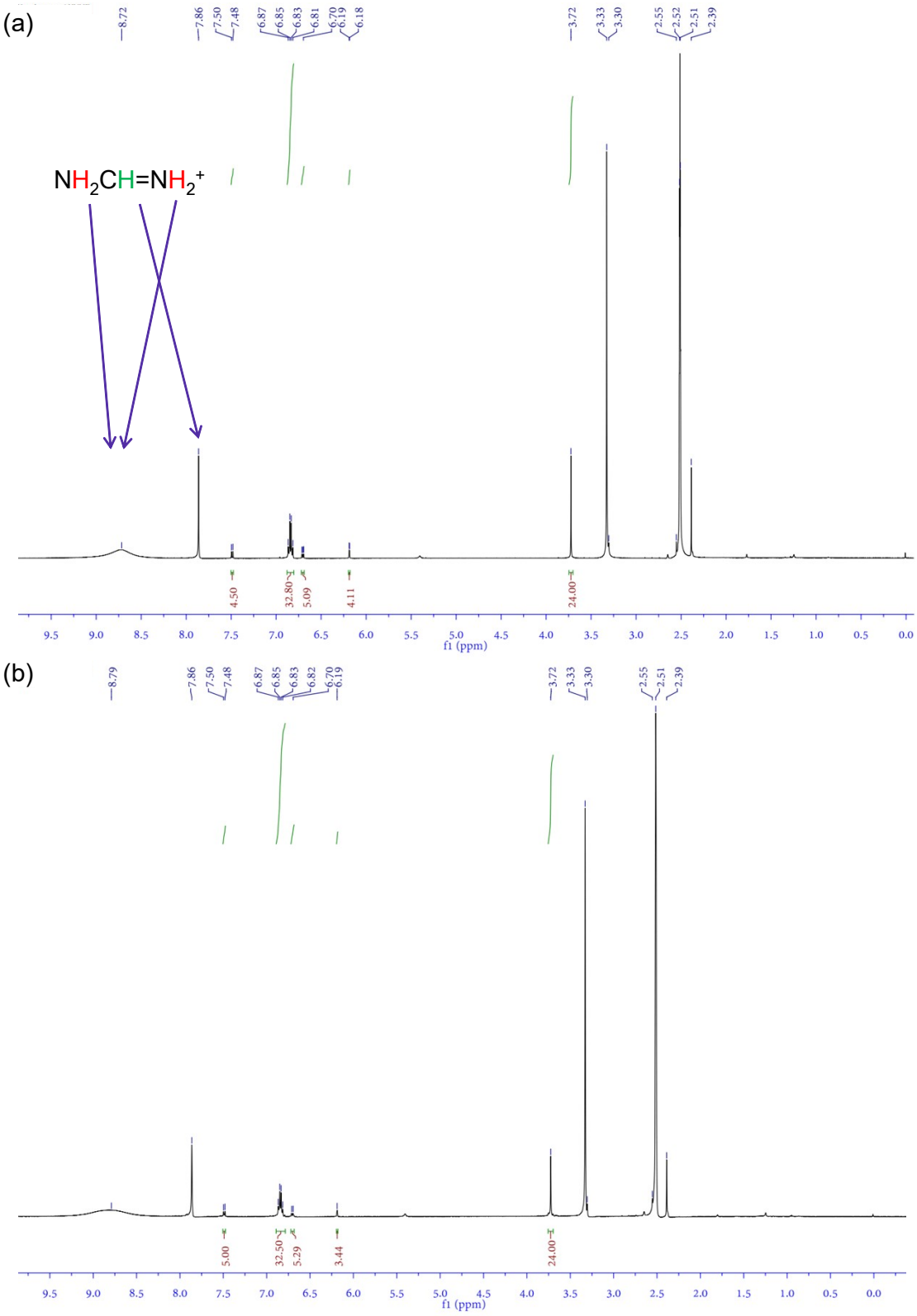

Figure S8. ^{1}H NMR spectra of the d_6-DMSO solutions derived from the digestion of the *spiro*-OMeTAD and perovskite films from the FTO|SnO_2|$Cs_{0.05}FA_{0.79}MA_{0.16}PbBr_{0.51}I_{2.49}$|HTL samples, HTLs deposited from the precursor solution based on (a) TeCA and (b) TeCA + BPO (90 mol.% BPO) and irradiated under 1-sun for 50s.

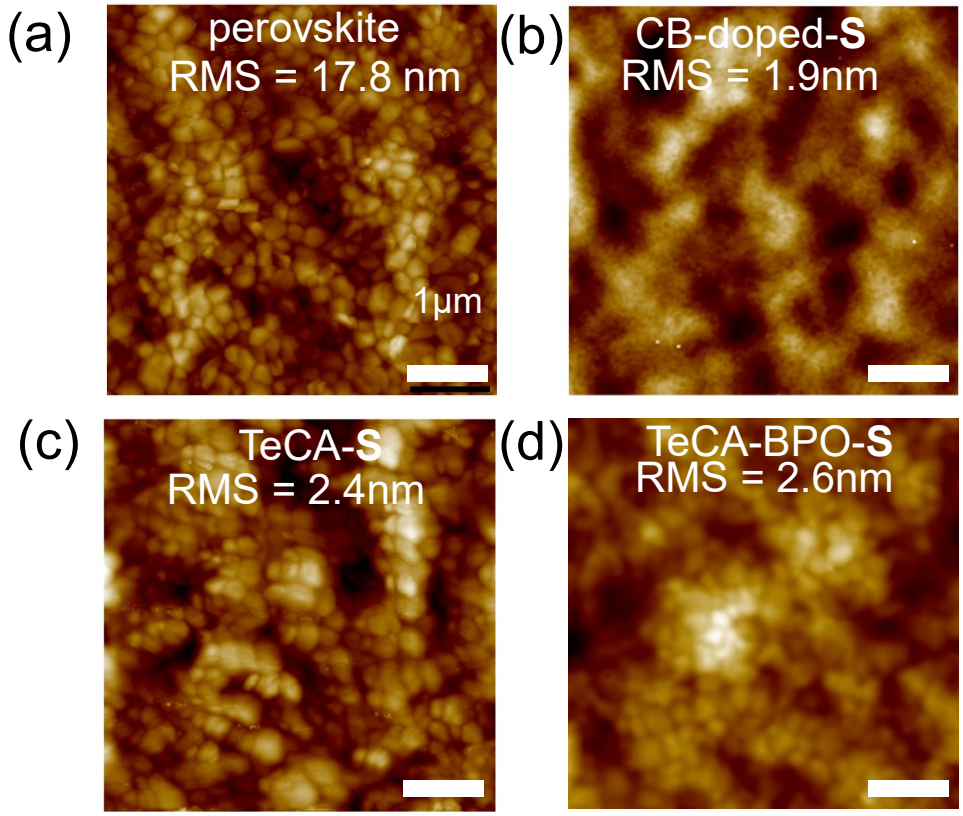

Figure S9. AFM images of the FTO|SnO_2|$Cs_{0.05}FA_{0.79}MA_{0.16}PbBr_{0.51}I_{2.49}$|HTL samples (a) without and (b-c) with different *spiro*-OMeTAD HTLs: (b) CB-**S** (60 mM); (c) TeCA-**S** (30 mM); (d) TeCA-BPO-**S** (90 mol.% BPO) (30 mM).

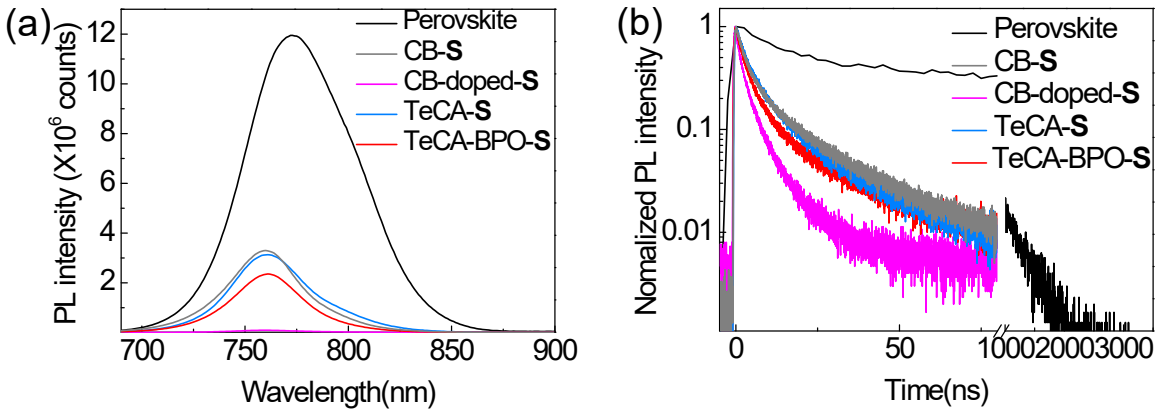

Figure S10. (a) Steady-state photoluminescence spectra and (d) time-resolved photoluminescence spectra the $Cs_{0.05}FA_{0.79}MA_{0.16}PbBr_{0.51}I_{2.49}$ perovskite on glass (*black*), and similar samples coated with different HTLs.

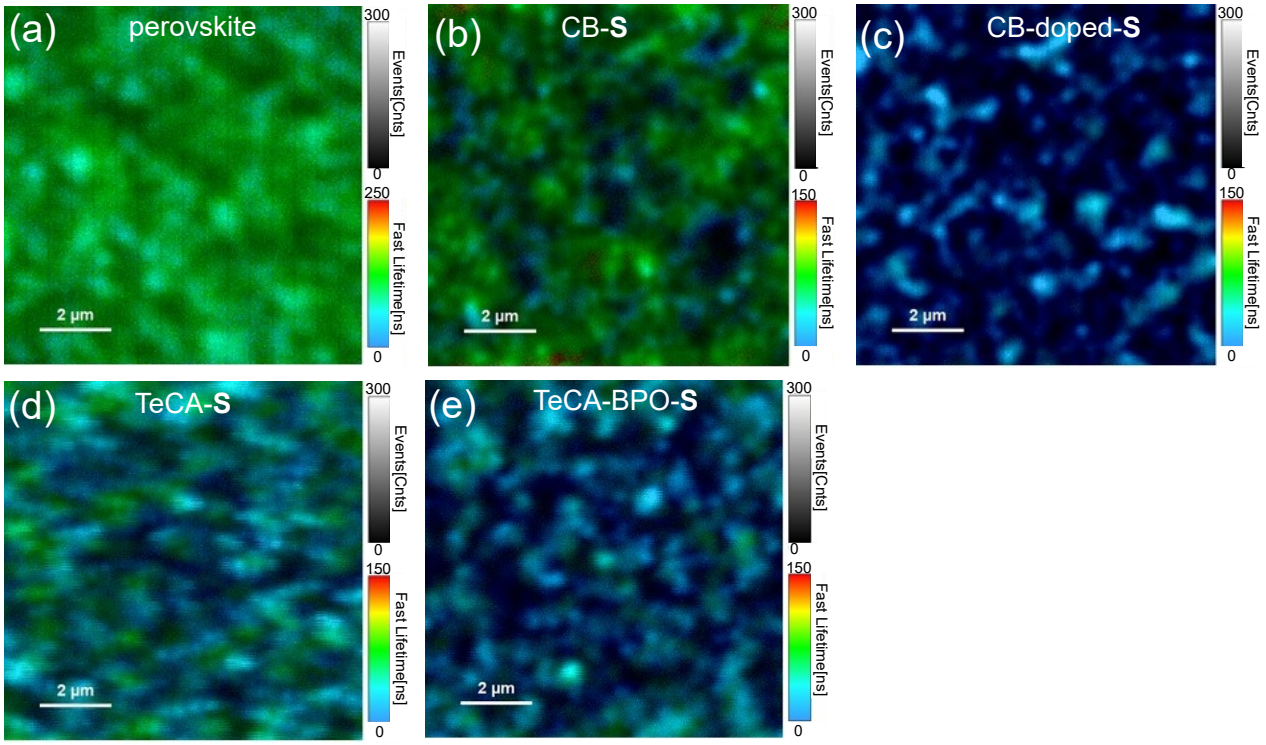

Figure S11. Time-resolved confocal PL lifetime maps of (a) the $Cs_{0.05}FA_{0.79}MA_{0.16}PbBr_{0.51}I_{2.49}$ perovskite film on glass, and perovskite covered with different HTLs (b) CB-**S**, (c) CB-doped-**S**, (d) TeCA-**S** and (e) TeCA-BPO-**S** (90 mol.% BPO).

Table S1. Parameters used to fit equation $Y=A_1\exp(-t/\tau_1) + A_2\exp(-t/\tau_1)+A_0$ to TPRL curves (**Figure 3b** in the main text) measured for the encapsulated $Cs_{0.05}FA_{0.79}MA_{0.16}PbBr_{0.51}I_{2.49}$ perovskite (on glass) without and with HTL deposited. The average PL lifetime $<\tau_{avg}>= \sum\alpha_i\tau_i$, where $\alpha_i= A_i\tau_i/\sum A_i\tau_i$

	A_1	τ_1(ns)	A_2	τ_2(ns)	τ_{avg}(ns)
perovskite	0.70	14.22	0.22	275.22	238.00
CB-**S**	0.76	3.42	0.25	18.66	13.25
CB-doped-**S**	0.68	1.62	0.33	6.40	5.99
TeCA-**S**	0.85	3.03	0.15	20.27	12.36
TeCA-BPO-**S**	0.97	2.96	0.09	21.30	10.30

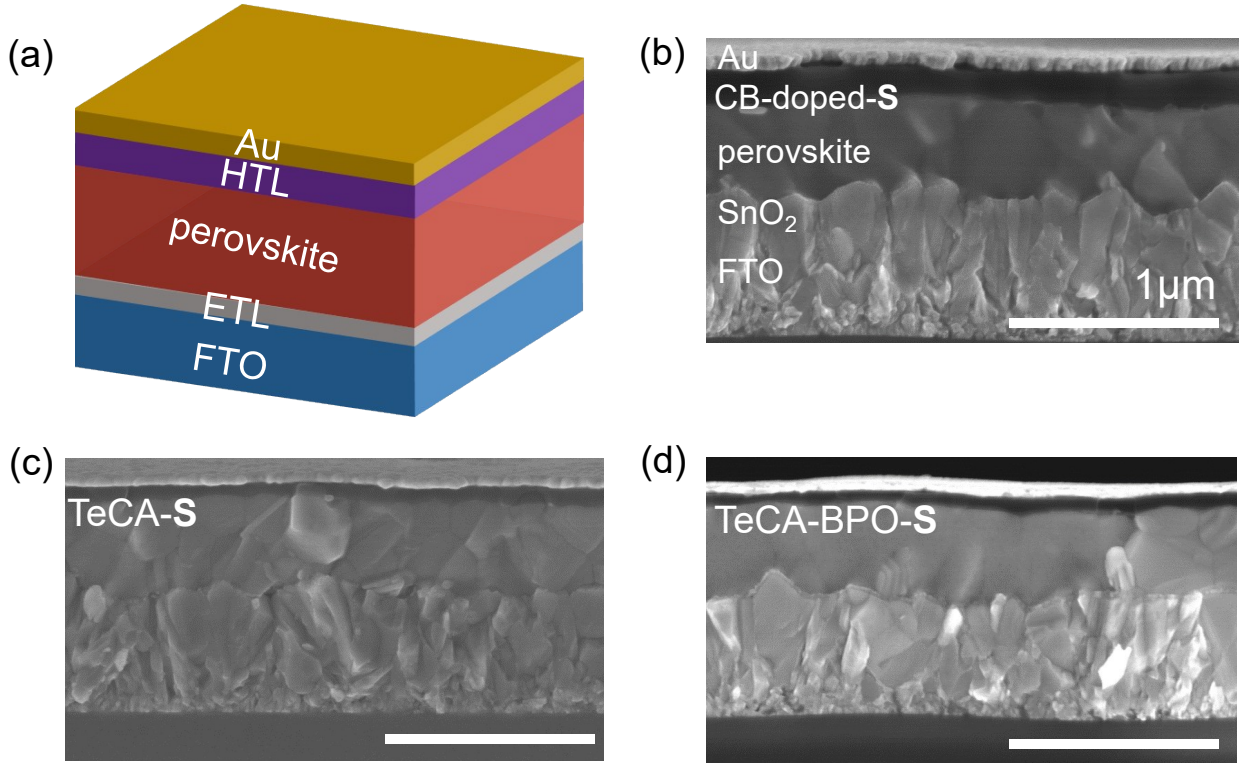

Figure S12. (a) Schematic diagram of solar cells with a standard *n–i–p* architecture. Cross-sectional SEM images for the solar cells with (b) CB-doped-**S**, (c) TeCA-**S** and (d) TeCA-BPO-**S** (90 mol.% BPO) HTLs.

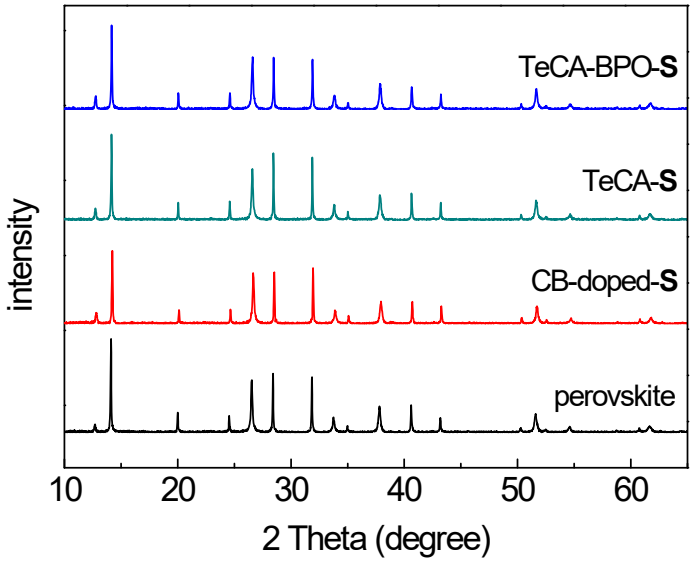

Figure S13. Full range XRD patterns for fresh $Cs_{0.05}FA_{0.79}MA_{0.16}PbBr_{0.51}I_{2.49}$ perovskite film (*black*) and fresh perovskite covered with different HTLs: CB-doped-**S** (*red*), TeCA-**S** (*dark cyan*) and TeCA-BPO-**S** (*blue*).

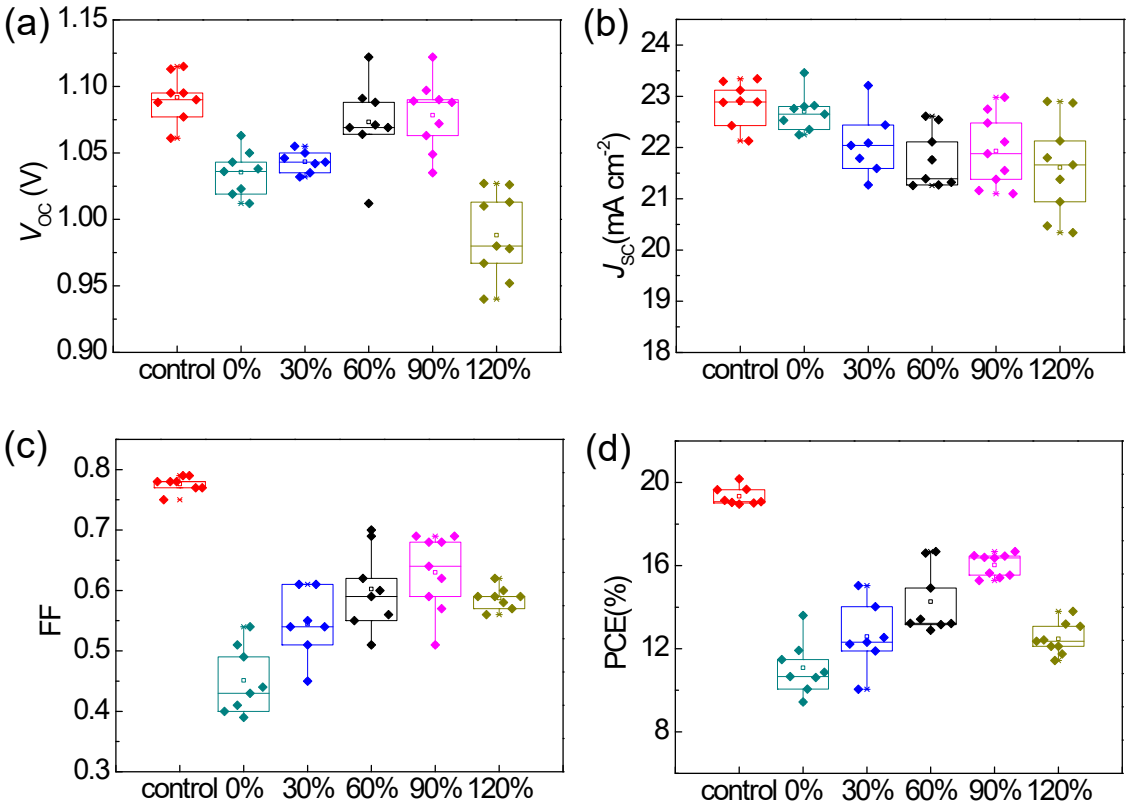

Figure S14. Statistics of photovoltaic parameters (a) V_{OC}, (b) J_{SC}, (c) FF and (d) PCE for the FTO|SnO_2|$Cs_{0.05}FA_{0.79}MA_{0.16}PbBr_{0.51}I_{2.49}$|i-BABr|HTL|Au solar cells using HTLs based CB-doped-**S** (control) and *spiro*-OMeTAD doped using TeCA+BPO combination with different amount of BPO added (mol.% with respect to *spiro*-OMeTAD). Concentration of *spiro*-OMeTAD in the precursor solution was 60mM. Solar cells performance parameters were determined from *J-V* curves, measured under 100 mWcm^{-2} simulated AM 1.5G solar irradiance with an aperture of 0.16 cm^2.

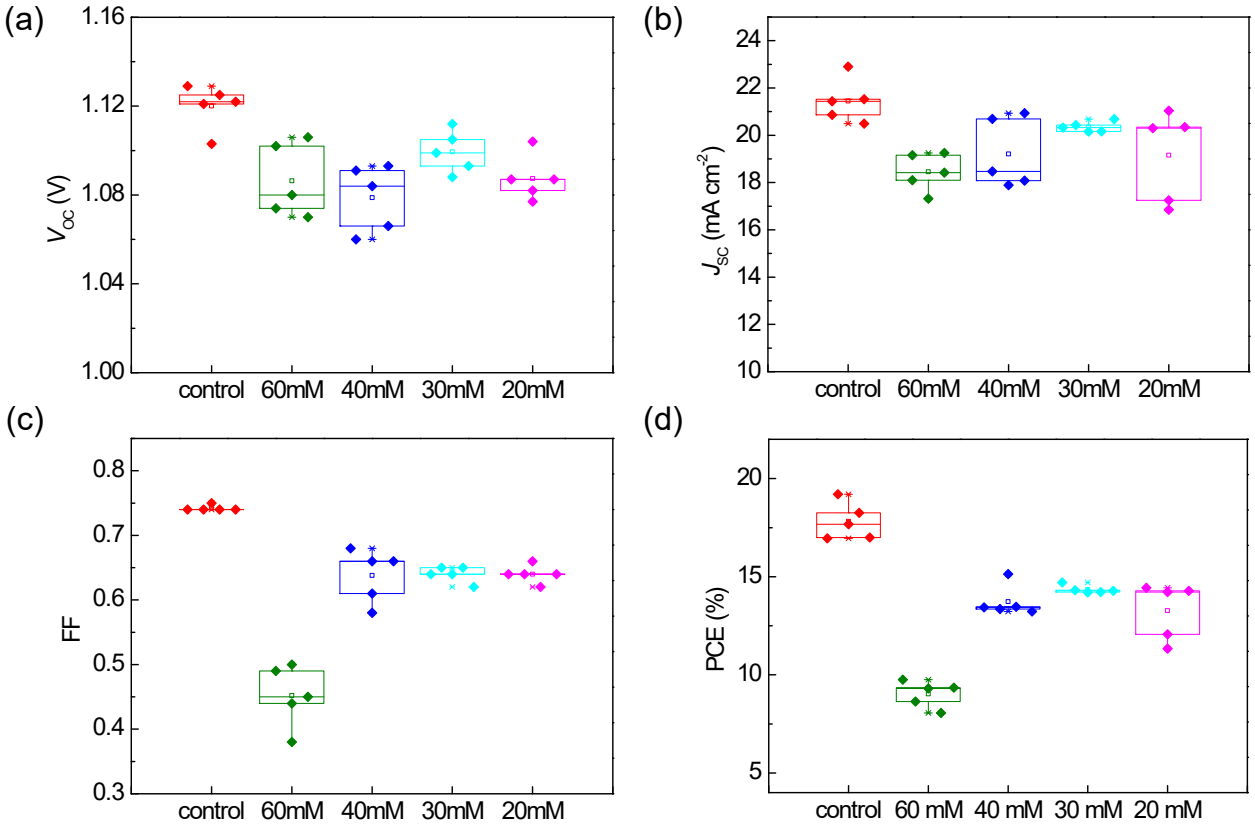

Figure S15. Statistics of the photovoltaic parameters (a) V_{OC}, (b) J_{SC}, (c) FF and (d) PCE for the FTO|SnO_2|$Cs_{0.05}FA_{0.79}MA_{0.16}PbBr_{0.51}I_{2.49}$|*i*-BABr |HTL|Au solar cells using HTLs based CB-doped-**S** (control) and *spiro*-OMeTAD doped using TeCA+BPO combination with different concentration of *spiro*-OMeTAD in the precursor solution. The amount of BPO is 90 mol.% with respect to *spiro*-OMeTAD. The photovoltaic parameters were extracted from *J-V* curves (FB to SC) measured under 100 mW/cm^2 simulated AM 1.5G solar irradiance with an aperture of 0.16 cm^2.

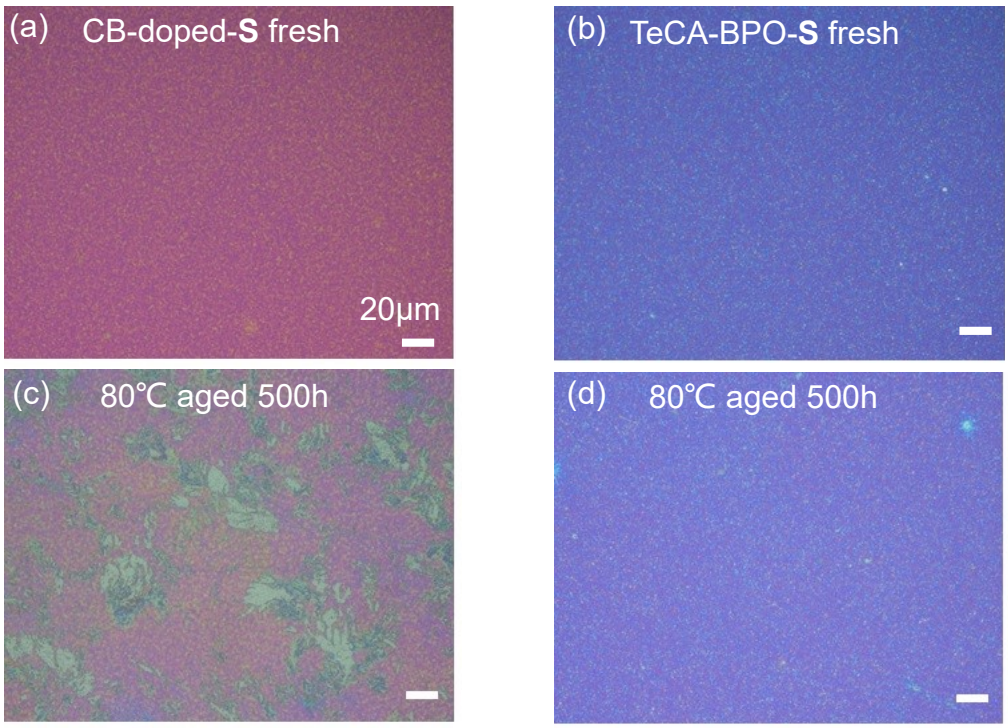

Figure S16. The visible light images of the fresh (a) CB-doped-**S**, (b) TeCA-BPO-**S** and aged (C) CB-doped-**S**, (d) TeCA-BPO-**S** HTL films. The films were not encapsulated and aged in an oven at 80 ℃ and at a relative humidity of 15 ± 5 % in air for 500 hours.

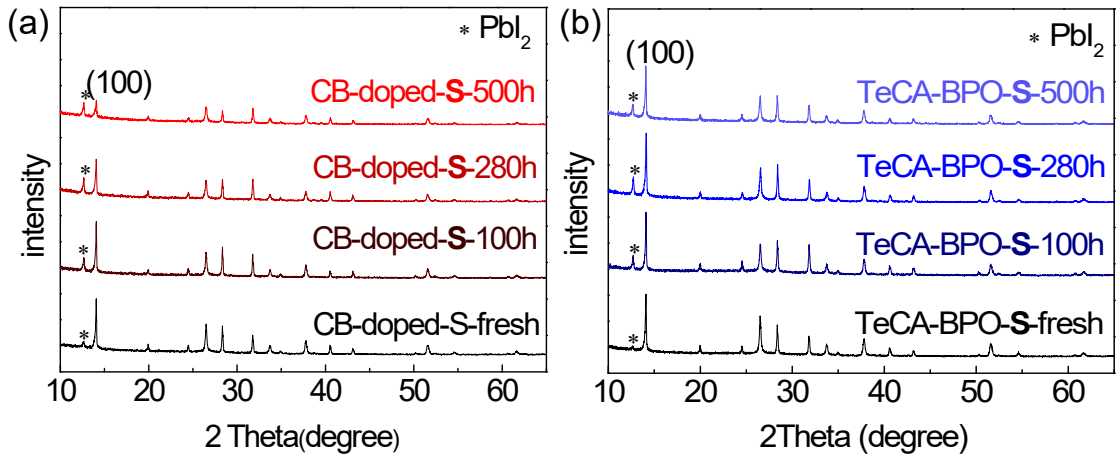

Figure S17. Evolution of XRD patterns of the non-encapsulated FTO|SnO_2|$Cs_{0.05}FA_{0.79}MA_{0.16}PbBr_{0.51}I_{2.49}$|i-BABr film covered with different HTLs at 80 °C and relative humidity of 15 ± 5% in air: (a) CB-doped-**S** (*red*) (b) TeCA-BPO-S (*blue*).

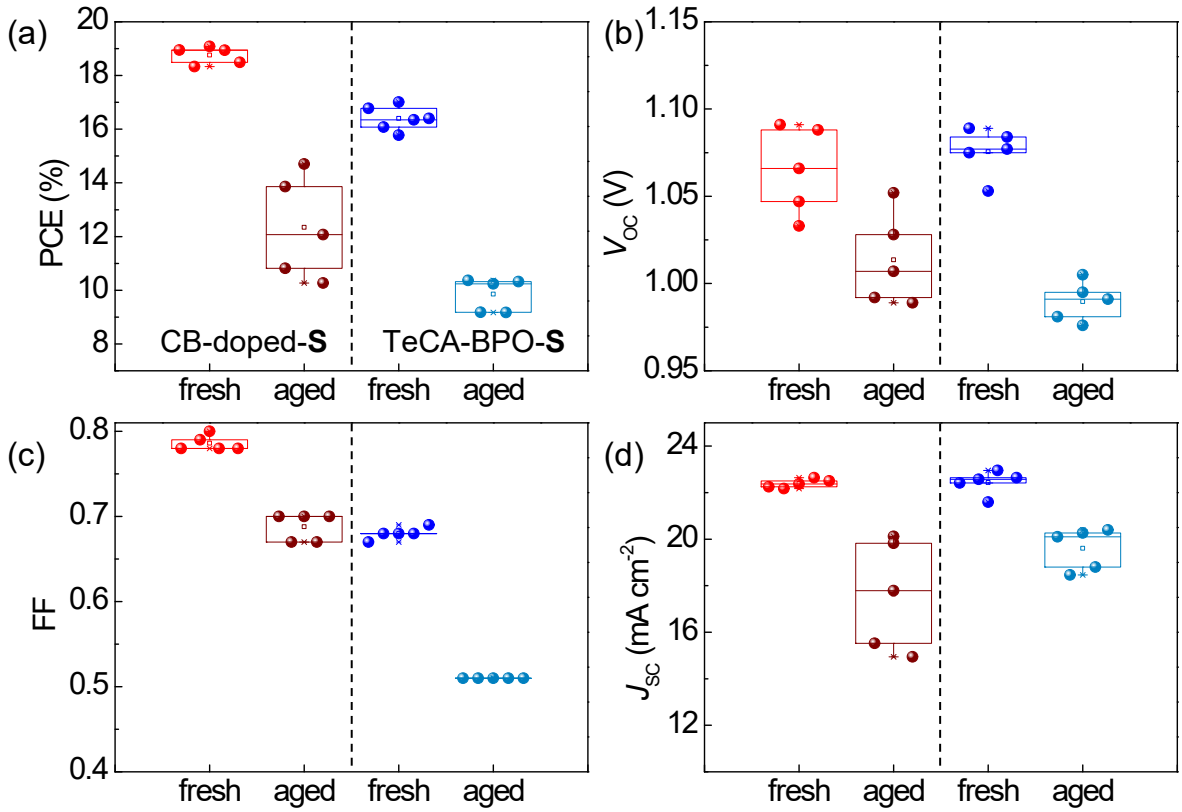

Figure S18. Performance of recorded under AM 1.5G 1-sun irradiation for non-encapsulated FTO|SnO_2|$Cs_{0.05}FA_{0.79}MA_{0.16}PbBr_{0.51}I_{2.49}$ | i-BABr | HTL | Au PSCs based on CB-doped-**S** and TeCA-BPO-**S** (90 mol.% BPO) HTLs during storage at relative humidity of 40 ± 5% in air for 5 days

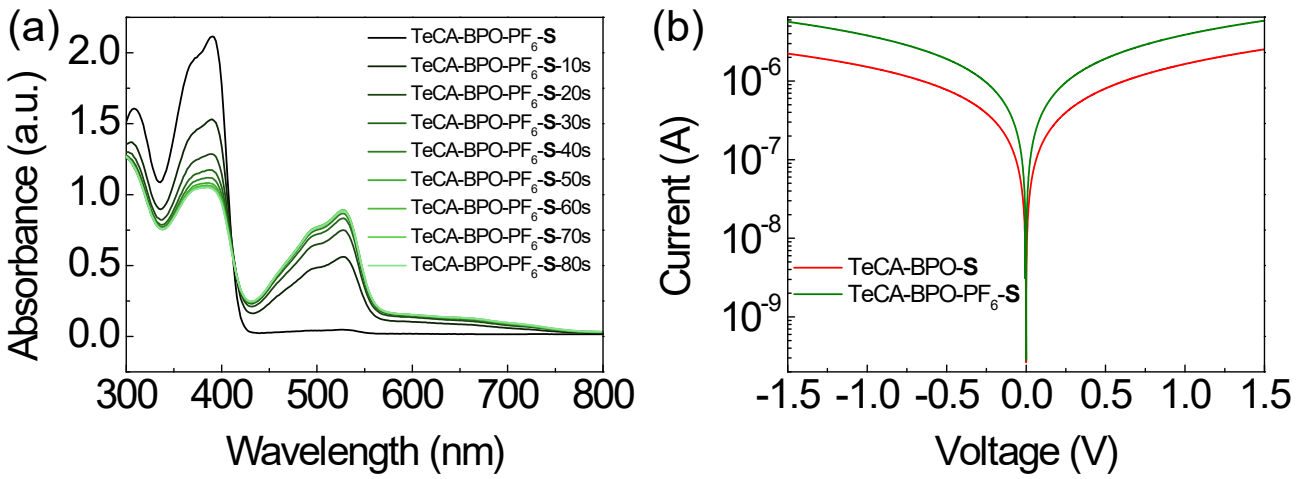

Figure S19. (a) Evolution of the UV−Vis absorption spectra of *spiro*-OMeTAD solutions with TeCA-BPO-PF_6; (b) I-V characteristics of spin-coated TeCA-BPO-**S** (*red*) and TeCA-BPO-PF_6-**S** (*gree*).

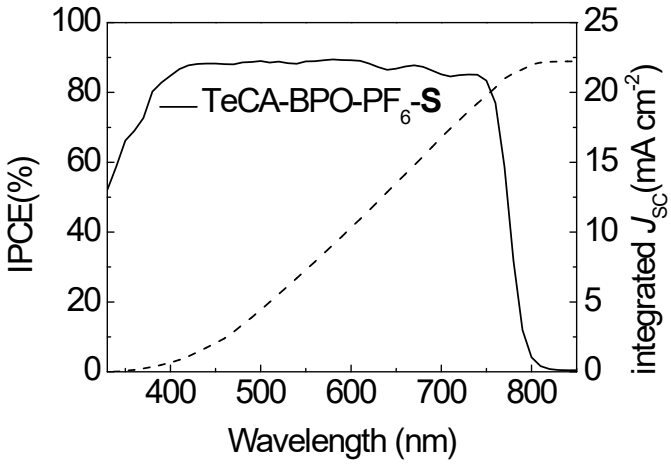

Figure S20. IPCE spectra and integrated current densities for the PSCs using TeCA-BPO-PF_6-**S** as HTM.

Table S2. Photovoltaic parameters [a] of the FTO|SnO_2|$Cs_{0.05}FA_{0.79}MA_{0.16}PbBr_{0.51}I_{2.49}$|i-BABr|HTL|Au under 1-sun simulated irradiation.

HTL			V_{OC} (V)	J_{SC} (mA cm^{-2})	FF	PCE (%)	q-SPO (%)	J_{IPCE} [b] (mA cm^{-2})
CB-doped-**S**	average FB to SC		1.11 ± 0.04	22.7 ± 0.5	0.80 ± 0.02	19.4±0.7		
	best	FB to SC	1.13	23.2	0.80	21.0	18.82	22.1
		SC to FB	1.07	23.1	0.76	18.7		
TeCA-**S**	average FB to SC		1.01 ± 0.07	22.3 ± 0.8	0.55 ± 0.03	12.3±1.7		
	best	FB to SC	1.08	22.5	0.58	13.9	11.92	21.8
		SC to FB	1.06	22.5	0.52	12.4		
TeCA-BPO-**S**	average FB to SC		1.11± 0.02	22.4 ± 1.1	0.72 ± 0.04	17.9±0.8		
	best	FB to SC	1.11	22.6	0.73	18.3	16.14	22.2
		SC to FB	1.07	22.7	0.60	14.4		
TeCA-BPO-PF6-**S**	average FB to SC		1.15 ± 0.02	22.9 ± 0.5	0.77 ± 0.01	20.5±0.6		
	best	FB to SC	1.16	23.1	0.79	21.1	19.76	22.2
		SC to FB	1.12	23.0	0.71	19.7		

[a] V_{OC} (open-circuit voltage), J_{SC} (short-circuit current density), FF (fill factor) and PCE (power conversion efficiency) data were derived from the *J-V* curves recorded for 10 devices of each type in the forward-bias (FB) to short-circuit (SC) direction, and for the best-performing devices recorded in each direction. Quasi steady-state power output (q-SPO) values were derived from the final point of 120 s measurements at fixed voltages corresponding to the maximum power points in the *J-V* data for the best-performing cell. All measurements were under AM 1.5G 1-sun simulated irradiation.

Reference:

1. T. l. Bu, J. Li, H. y. Li, C. Tian, J. Su, G. Tong, L. K. Ono, C. Wang, Z. p. Lin, N. y. Chai and *Science*, 2021, **372**, 1327-1332.